Feature Article

Simultaneous Imaging of Exhaust Gas Residuals and Temperature During HCCI Combustion

David A Rothamer

This article focuses on a new diagnostic technique that has been developed to study the influence of the exhaust gas residuals and temperature distributions on homogeneous-charge compression-ignition (HCCI) combustion. The technique utilizes two-wavelength excitation of a fluorescence tracer species (3-pentanone) to take high-fidelity snapshots of the in-cylinder distributions of EGR and temperature inside firing optical engines. The development of the diagnostic was moti-vated by the need to understand the influence of in-cylinder mixture stratification on the HCCI combustion process.

Introduction

Homogeneous-charge compression-ignition engines offer the potential for significantly reduced nitric oxide (NO_x) and soot emissions while still competing with their Diesel counterparts in terms of efficiency[1]. The main drawbacks for the combus-tion strategy are the limited engine load and speed range and the lack of direct control of combustion initiation. Various strategies to overcome these limitations have been suggested, and many of the strategies utilize large levels of internal EGR and stratification of the in-cylinder composition and temperature distribution[1-6]. The success of these strategies relies on the ability to create and control the level of stratification, to understand this process requires spatially resolved diagnostics to monitor the levels of EGR and temperature stratification in-cylinder.

The need to measure the in-cylinder distributions of EGR and temperature has motivated the develop-ment of a diagnostic capable of simultaneous imag-ing of EGR and temperature during HCCI combus-tion. The diagnostic utilizes two readily available fixed wavelength pulsed laser systems along with a dual-frame interline-transfer intensified CCD cam-era to capture images of fluorescence from a tracer molecule which is added to the intake air and fuel. The fluorescence images can be converted to tem-perature and EGR utilizing appropriate corrections to the data. The diagnostic has been optimized to give the best possible measurement precision over a wide range of temperature and pressure conditions relevant for HCCI combustion. This article gives an overview of the diagnostic and presents results ac-quired for two different HCCI combustion strategies.

Overview of Two-Wavelength EGR and Temperature Imaging Diagnostic

Tracer-based Planar Laser-Induced Fluorescence (PLIF) was chosen as the diagnostic technique for this work. Tracer-based PLIF utilizes a fluorescence tracer with easily accessible absorption and emis-sion bands to make measurements in flow environ-ments. Temperature measurements have been per-formed previously using tracer-based PLIF by Einecke et al.[7], Fujikawa et al.[8], Kakuho et al.[9], and others. A dual excitation wavelength ap-proach was chosen for measuring temperature. In this approach two fluorescence images are acquired sequentially with two different laser excitation wavelengths. The time between the two images is short enough to freeze the flow motion, in this case 5 μs. The acquired images are corrected for back-ground signal and laser sheet non-uniformities, then the ratio of the two images is taken. The resulting ratio can be a strong function of temperature with appropriate choice of tracer and excitation wave-lengths. The resulting signal ratio can then be re-lated directly to temperature.

Dual wavelength excitation was performed with

3-pentanone as the chosen fluorescence tracer. 3-pentanone was chosen due to its resistance to fluo-rescence quenching by oxygen and its relatively broad absorption spectrum shown in Figure 1. The broad absorption allows for excitation with a wide variety of laser sources. The absorption cross sec-tion of 3-pentanone increases substantially with in-creasing temperature for excitation wavelengths greater than 270 nm. This feature counteracts de-creases in fluorescence quantum yield at high tem-peratures allowing for imaging at temperatures close to 1000 K with longer excitation wavelengths.

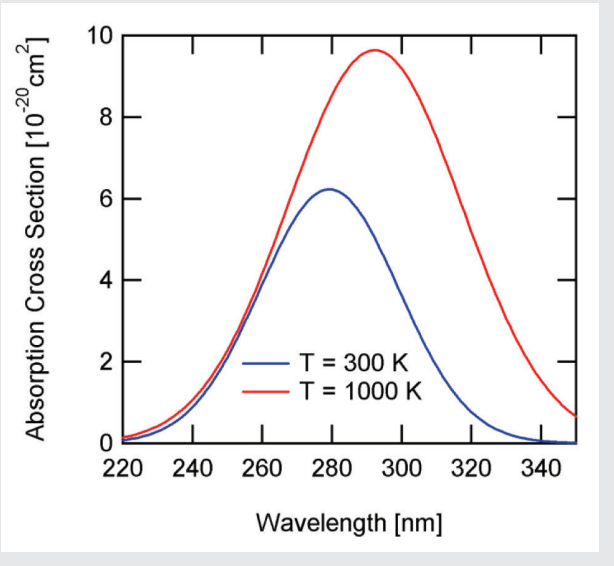

Figure 1 3-pentanone absorption spectrum for two different temperatures calculated using the curve fit of Koch[10].

Measurements of the EGR distribution are made using either of the 3-pentanone fluorescence images acquired for the temperature measurement. Because tracer is added into both the intake air and the fuel the 3-pentanone fluorescence signal gives a meas-urement of the local air-plus-fuel mole fraction. The in-cylinder contents can be idealized as consisting of just three components, air, fuel, and EGR, by measuring any two of these components we can de-termine the third. If all of the tracer is consumed during the combustion process then the EGR mole fraction is determined by subtraction of the air-plus-fuel mole fraction image from 1, i.e.,

$$\chi_{EGR} = 1 - (\chi_{Air} - \chi_{Fuel}) \quad \cdots\cdots\cdots\cdots\cdots\cdots\cdots\cdots \quad (1)$$

where χ_{EGR} is the EGR mole fraction, χ_{Air} is the air mole fraction, and χ_{Fuel} is the fuel mole fraction. A similar technique was used previ-ously by Deschamps and Baritaud[11] to make EGR measurements and was refer to by them as negative PLIF (N-PLIF).

Optimization of Diagnostic for Engine Pressures and Temperatures

Small temperature differences and composition dif-ference can strongly influence the ignition and heat release process for HCCI combustion[5]. Because of this it was desired to have the best possible single laser pulse (single-shot) precision for both the tem-perature and EGR measurements. If fluorescence signals are relatively high and the detection statis-tics are shot-noise limited, then the fluorescence signal-to-noise SNR ratio is proportional to the square root of the fluorescence signal. Therefore, to maximize SNR and improve precision, the fluores-cence signal needs to be maximized over the range of engine conditions of interest. Fluorescence signal in the linear excitation limit is given by:

$$S_f = \frac{E}{h\nu} dV_c \frac{\chi_{abs} P}{kT} \sigma(\nu,P,T,\chi_i) \phi(\nu,P,T,\chi_i) \eta_{col} \quad \cdots\cdots \quad (2)$$

where S_f is the number of fluorescence photons collected, E is the laser energy per a pulse, h is Planck's, ν is the frequency of the exciting photons, χ_{abs} is the absorbing species mole fraction, P is the pressure, T is the temperature, σ is the absorp-tion cross section, ϕ is the fluorescence quantum yield, and η_{col} is the collection efficiency of the optics system.

Based on Equation 2, to maximize the signal levels for a specific tracer with respect to the excitation wavelength the product $\sigma\phi/\nu$ needs to be maxi-mized. Not all excitation wavelengths were consid-ered in the optimization process. Instead, only wavelengths corresponding to high pulse energy laser systems or Raman-shifted wavelengths gener-ated by these systems were considered. These sys-tems included krypton fluoride (KrF) excimer lasers at 248 nm, the 4th harmonic of Nd:YAG lasers at 266 nm, the output of xenon chloride (XeCl) la-sers at 308 nm, and the output of xenon fluoride (XeF) lasers at 351 nm.

Models for fluorescence quantum yield and absorp-tion cross section were used to estimate temperature and EGR precision over the range of in-cylinder conditions of interest. Figure 2(a) and 2(b) show the results of these calculations for the optimal excita-tion wavelength combination of 277 nm and 308 nm for single-shot imaging. The 277 nm wavelength is generated through Raman shifting the output of a 248 nm KrF laser in high pressure hydrogen. The resulting EGR and temperature uncertainties are for a specific experimental setup. Further improve-ments can be made with changes in experimental parameters such as increasing the level of pixel binning.

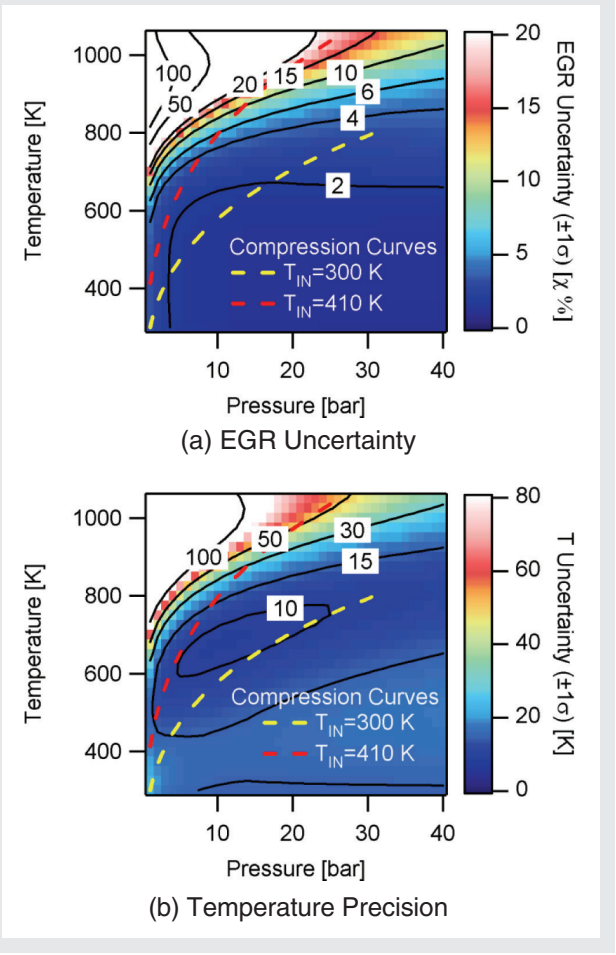

Figure 2 (a) EGR uncertainty for 277 nm and 308 nm wavelength combination
(b) Temperature uncer-tainty for 277 nm and 308 nm wavelength combina-tion.

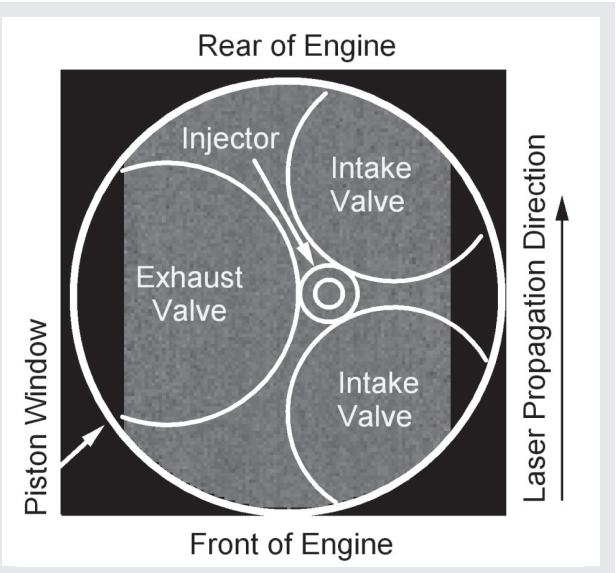

Figure 3 Sample uniform PLIF image with valve locations and injector location superimposed.

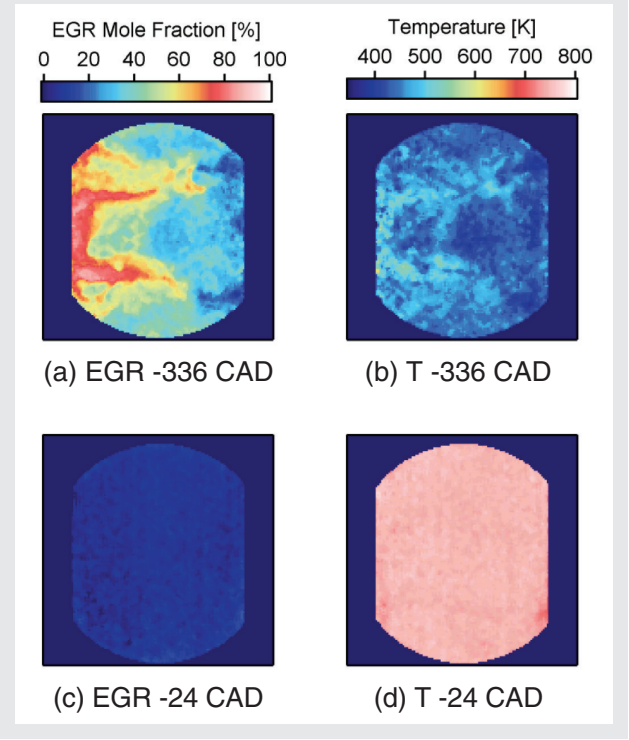

Figure 4 Simultaneous images of EGR and tempera-ture taken immediately after intake valve opening (-336 CAD) and close to top dead center of compres-sion (-24 CAD) for pure HCCI operation.

Simultaneous Measurements of EGR and Temperature during HCCI Combustion

The developed diagnostic has been applied to two different HCCI combustion strategies. The first of these two strategies was pure HCCI using a uniform mixture of air and n-heptane at a low equivalence ratio of 0.30. The second strategy studied was HCCI with negative valve overlap and direct fuel injection. This strategy utilizes the retention of high levels of internal EGR to heat the incoming air-fuel mixture and provide significant dilution, allowing for opera-tion at an equivalence ratio of 0.8.
Figure 3 shows a sample PLIF image of a uniform mixture in-cylinder. The image has the locations of the intake valves and exhaust valve superimposed along with the injector location. The laser sheets used for excitation propagate from the bottom of the image to the top.

Imaging results for pure HCCI combustion are shown in Figure 4. The overall level of EGR in-cylinder was approximately 8% for pure HCCI op-eration. The images have a spatial resolution of 0.5 mm and have a 3×3 median filter applied which decreases noise while maintaining

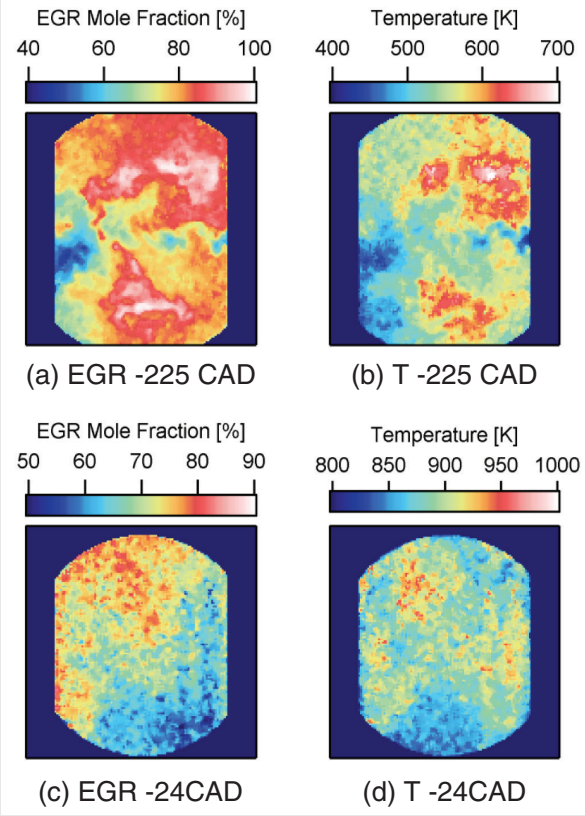

Figure 5 Simultaneous images of EGR and tempera-ture taken at -225 CAD (45 CAD BBDC) and close to top dead center of compression at -24 CAD (24 CAD BTDC) for NVO operation.

spatial resolution[12]. Figures 4(a) and (b) show the EGR and tem-perature distributions at -336 CAD which is 24 CAD after the intake valves start opening. At this time the EGR and temperature distributions are highly non-uniform with local levels of EGR ap-proaching 100%. At the image timing near ignition shown in Figure 4(c) and (d) the mixture is close to uniform with the low level EGR uniformly distrib-uted throughout the mixture.

For NVO operation the intake and exhaust valve timings are significantly different than the relatively standard timings used for pure HCCI operation. In particular, the exhaust valve closes at 276 CAD (84 CAD BTDC) trapping a substantial amount of ex-haust gases in-cylinder. Approximately 30% of the fuel is injected during this negative valve overlap and some heat release occurs. The intake valves open late at -297 CAD (63 CAD ATDC). The late intake opening results in large amounts of EGR still present in the image of Figure 5(a) even though the intake valve has been open for 72 CAD. The simul-taneous temperature image of Figure 5(b) shows a corresponding stratification in the temperature dis-tribution. At late image timings right before TDC the in-cylinder mixture is still quite non-uniform as shown in Figure 5(c) and (d). Non-uniformities are present in both the EGR and temperature distribu-tions. However, the correlation of high EGR with high temperature seems to be less near TDC.

Conclusion

The image results show the capability of the diag-nostic to capture EGR and temperature distributions under a wide variety of in-cylinder conditions. The developed diagnostic was optimized to be able to image under this wide variety of in-cylinder condi-tions through careful selection of the tracer and ex-citation wavelength used for tracer-based negative PLIF of EGR and temperature. Future work will focus on further optimization for specific conditions such as high in-cylinder pressure and high tempera-ture at modest in-cylinder pressures.

References

[1] J.E. Dec, M. Sjöberg, SAE Technical Paper 2004-01-0557.
[2] T. Amano, S. Morimoto, S. Kawabata, SAE Technical Paper 2001-01-1024.
[3] T. Noda, D.E. Foster, SAE Technical Paper 2001-01-0250.
[4] A. Kakuho, M. Nagamine, Y. Amenomori, T. Urushihara, T. Itoh, SAE Technical Paper 2006-01-1202.
[5] M. Sjöberg, J.E. Dec, N.P. Cernansky, SAE Technical Paper 2005-01-0113.
[6] R.E. Herold, D.E. Foster, J.B. Ghandhi, R.J. Iverson, J.A. Eng, P.M. Najt, Int. J. Engine Res. 8 (3) (2007) 241-257.
[7] S. Einecke, C. Schulz, and V. Sick, Applied Physics B-Lasers and Optics, 71 (5):717-723, 2000.
[8] T. Fujikawa, K. Fukui, Y. Hattori, and K. Aki-hama, SAE Technical Paper 2006-01-3336.
[9] A. Kakuho, M. Nagamine, Y. Amenomori, T. Urushihara, and T. Itoh, SAE Technical Paper 2006-01-1202.
[10] J. Koch, Personal communication, 12/2007.
[11] B. Deschamps and T. Baritaud, SAE Technical Paper 961928.
[12] J.B. Ghandhi, Exp. Fluids 40 (4) (2006) 577-588.

David A Rothamer
University of Wisconsin-Madison
Mechanical Engineering Department